Desalination and Water Treatment
www.deswater.com

doi: 10.5004/dwt.2018.21626

106 (2018) 116–124
February

Solvothermal synthesis of carbon nanotubes/Bi_2WO_6 composites to improve photocatalytic activity of Bi_2WO_6

Chao-Yin Kuo[a], Chung-Hsin Wu[b,*], Ming-Ju Hsu[b]

[a]*Department of Environmental and Safety Engineering, National Yunlin University of Science and Technology, Yunlin, Taiwan, Tel. 886-5-5347311, email: kuocyr@ms35.hinet.net (C.-Y. Kuo)*
[b]*Department of Chemical and Materials Engineering, National Kaohsiung University of Science and Technology, 415 Chien Kung Road, Kaohsiung, Taiwan, Tel. 886-7-3814526, Fax 886-7-3830674, email: wuch@nkust.edu.tw (C.-H. Wu), Tel. 886-938152172, email: chute514@gmail.com (M.-J. Hsu)*

Received 14 July 2017; Accepted 11 November 2017

ABSTRACT

In this investigation, the solvothermal process is utilized to synthesize carbon nanotubes (CNTs)/Bi_2WO_6 (BW) composites. The photocatalysis percentage of C.I. Reactive Red 2 (RR2) was used to compare the photocatalytic activity of the prepared CNTs/BW composites. The surface characteristics of the prepared CNTs/BW composites were elucidated by X-ray diffractometry, scanning electron microscopy, transmission electron microscopy (TEM), specific surface area analysis, zeta potential analysis, UV-vis spectrophotometry, X-ray photoelectron spectroscopy and fluorescence spectrophotometry. The optimal CNTs dopant dosage in BW was that associated with C/B molar ratio = 1 and the photocatalyst thus formed, denoted as 1CBW, had a specific surface area, pH at zero charge and band gap of 84.1 m^2/g, 4.6 and 3.1 eV, respectively. A high-resolution TEM image of 1CBW revealed a very tight interface between the CNTs and BW in the composites, which formed a heterojunction. The rates of RR2 photocatalysis by CNTs/BW composites under solar and visible-light both followed a pseudo-first-order kinetic model. The solar photocatalysis and visible-light photocatalysis rate constants for the removal of RR2 by BW were 2.86 and 0.234 h^{-1}, respectively, and by 1CBW were 5.24 and 0.438 h^{-1}, respectively. This study demonstrated that the recombination of photo-generated electron-hole pairs in BW is greatly inhibited by the introduction of CNTs, revealing that the separation of photo-generated electron-hole pairs in 1CBW is more efficient than in BW.

Keywords: Solvothermal; Carbon nanotubes; Bi_2WO_6; Solar; Visible-light; Photocatalysis

1. Introduction

Bismuth tungstate, Bi_2WO_6 (BW), the simplest member of the Aurivillius family and a potential visible-light photocatalyst, has a layered structure with perovskite-like slabs of WO_6 and $[Bi_2O_2]^{2+}$ layers; it was first studied by Kudo and Hijii [1]. However, pure BW has low photoactivity owing to its rapid photo-induced electron-hole recombination and relatively narrow absorption region [2–4]. Therefore, its photocatalytic efficiency must be improved to make it suitable for practical applications.

Various carbon materials, including activated carbon (AC), carbon black, graphite, and carbon nanotubes (CNTs), are important in heterogeneous catalysis as either catalysts or catalyst supports [5]. CNTs show high chemical and thermal stability, a large surface area, excellent electron conducting ability and well-defined hollow interiors, so they are potential supports for nanocomposites [6–8]. In the search for new tools to enhance the photoactivity of photocatalysts, recent studies have focused on CNTs-based nanocomposites owing to their unique properties and promising applications. Numerous photocatalytic systems that are based on the CNTs have been examined and their activity

*Corresponding author.

has been increased, such as TiO_2 [6,8–11], CdS [12], $Bi_4O_5Br_2$ [13], $BiVO_4$/BW [14], $InVO_4$ [15], C_3N_4 [16], BW [17], $BiVO_4$ [18], and $ZnFe_2O_4$ [19]. Lin et al. [14] prepared CNTs/$BiVO_4$/BW nanocomposites to enhance the photocatalytic performance of BW. The introduction of CNTs prevented the agglomeration of nanocomposites, expanded the range of absorption of visible light, and favored the effective separation of photo-induced electron-hole pairs [18]. Zhang et al. [15] showed that CNTs/$InVO_4$ nanofibers exhibited greater photocatalytic activity in Rhodamine B (RhB) degradation than did pure $InVO_4$ nanofibers, perhaps because of the role of CNTs as electron transporters and acceptors in the composites. Such enhancements have been attributed to the high mechanical strength, hollow and layered structure, large specific surface area with excellent adsorption properties and electrical conductivity of CNTs [15,20,21]. Chen et al. [20] and Xu et al. [21] suggested that CNTs could be used as electron reservoirs to inhibit the recombination of the electron-hole pairs and thereby increase the photocatalytic activity of CNTs-based nanocomposites.

Several studies have used carbon-based materials to improve the photocatalytic activity of BW. Li et al. [22] indicated that the photocatalytic performance of BW was greatly enhanced by adding carbon up to a certain amount, but the photoactivity of C/BW was reduced when excess glucose was used in the synthesis. They found that the presence of a small amount of AC (nominal content of 2 wt%) increased surface area and visible-light absorption while reducing the band gap of BW, significantly improving its photocatalysis of RhB and phenol [23]. Modifying BW with the appropriate amount of reduced graphene oxide (RGO) significantly improves its degradation of RhB, phenol and Cr(VI) pollutants. RGO facilitates the transfer of photo-induced electrons in BW to model materials, significantly improving its photocatalytic performance [24]. Min et al. [25] found that the photocatalytic activity of graphene/BW markedly exceeded that of pure BW. Chen et al. [26] revealed that the photocatalytic performance of BW was enhanced greatly by the doping with carbon microspheres. Yue et al. [17] utilized the hydrothermal method to synthesize CNTs/BW, which exhibited greater photocatalytic degradation of tetracycline than pure BW. The surface properties of BW varied with the method of synthesis. Accordingly, the optimal dosage of carbon-based materials for modifying the surface of BW varied with the method of preparation. The solvothermal route gained the benefits of hydrothermal and sol-gel methods. Hence, solvothermal process allowed for the precise control over the crystallinity and size of photocatalysts. To the best of our knowledge, the use of the solvothermal method to synthesize the CNTs/BW composites has not been investigated. Hence, in this study, ethylene glycol (EG) is used as a solvent to synthesize CNTs/BW composites. The photocatalytic activity of the prepared CNTs/BW in the photocatalysis of C.I. Reactive Red 2 (RR2) was evaluated. The objectives of this study were (i) to determine the effects of CNTs dosage on the photocatalytic activity of CNTs/BW composites under solar and visible-light; (ii) to measure the surface characteristics of prepared CNTs/BW composites; and (iii) to identify the major oxidative species in the CNTs/BW system.

2. Materials and methods

2.1. Materials

Bismuth (III) nitrate ($Bi(NO_3)_3{\cdot}5H_2O$) and sodium tungstate ($Na_2WO_4{\cdot}2H_2O$) were used as precursors in the formation of Bi and W, respectively, which were used to generate BW and CNTs/BW composites (Katayama, Japan). RR2 ($C_{19}H_{10}Cl_2N_6Na_2O_7S_2$) was purchased from Sigma Aldrich (USA). Sodium nitrite ($NaNO_2$) and EG were used as an ultraviolet-light (UV) cut-off agent and a solvent in the solvothermal process, respectively; both were obtained from Katayama. The CNTs used herein were multi-wall nanotubes (CBT, MWNTs-2040). These CNTs were manufactured by the pyrolysis of methane gas on Ni particles via chemical vapor deposition. The C, O and Ni contents in the CNTs were 90.6%, 8.1% and 1.3%, respectively. Their surface area, average pore diameter and pore volume were 82.2 m^2/g, 2.5 nm and 1.07 cm^3/g, respectively [27]. The CNTs were 5–15 μm long and the mass proportion of amorphous carbon in CNTs was less than 2%. To detect the active species that formed in the CNTs/BW system, superoxide radicals, holes and hydroxyl radicals were quantified by adding K_2CrO_4 (Katayama), ethylenediaminetetraacetic acid disodium salt (EDTA-2Na) (Katayama) and isopropanol (IPA) (J.T. Baker, USA), respectively. The pH of solution was adjusted by adding 0.1 M HNO_3 or NaOH during the reaction; both of these reagents were purchased from Merck (USA). All materials were used as received without further purification. All solutions were prepared using deionized water (Milli-Q) and reagent-grade chemicals.

2.2. Preparations of BW and CNTs/BW composites

BW was prepared under conditions that were identified as optimal by Wu et al. [28]. 1.319 g $Na_2WO_4{\cdot}2H_2O$, 3.881 g $Bi(NO_3)_3{\cdot}5H_2O$ and the desired amount of CNTs (0.024, 0.048 and 0.096 g) were added to 70 mL EG and the resulting solution was vigorously magnetically stirred, yielding C/W molar ratios of 0.5, 1 and 2. The mixtures were adjusted to pH 2 by adding 10 M NaOH with stirring for 1 h. The mixtures were sealed in a 100 mL Teflon-lined stainless steel autoclave and heated at 433 K under self-generated pressure for 12 h; they then cooled naturally to room temperature. The precipitates were collected by filtration and washed using 50 mL 95% ethanol and 100 mL D.I. water to remove any residual impurities. The samples were finally dried in air at 333 K for 24 h. The samples with C/W molar ratio of 0.5, 1 and 2 for CNTs/BW were denoted as 0.5CBW, 1CBW and 2CBW, respectively. The C/W molar ratios of 0.5, 1 and 2 were equivalent to CNTs/BW weight ratios of 0.86%, 1.72% and 3.44%, respectively.

2.3. Characterization of CNTs/BW composites

The phase structure of CNTs/BW composites was analyzed using an X-ray diffractometer (Bruker D8 SSS, Germany) with CuKa radiation (40 kV, 30 mA) over the 2q range of 20°–80°. The surface charge of CNTs/BW composites in aqueous solution was measured using a zeta potential analyzer (BIC 90 plus, USA), and used to calculate the pH of the zero point of charge (pH_{zpc}). The morphology and

microstructure of the CNTs/BW composites were characterized by scanning electron microscopy (SEM) (JEOL 6330 TF, Japan) and transmission electron microscopy (TEM) (JEOL 3010, Japan). Diffuse reflectance UV-vis spectra of CNTs/BW composites, obtained using a UV-vis spectrophotometer (JAS.CO-V670, Japan), were used to calculate the band gap. The Brunauer-Emmett-Teller (BET) specific surface area, pore diameter, and pore volume of CNTs/BW composites were obtained using a Micromeritics ASAP 2020 system (USA). The photoluminescence (PL) spectra were used to examine the efficiency of charge carrier transfer and separation because PL emission is caused by the recombination of photo-induced electron-hole pairs. The PL spectra of the samples were obtained at room temperature using a fluorescence spectrometer (Hitachi F-4500, Japan) at an excitation wavelength of 300 nm from a xenon lamp. The X-ray photoelectron spectroscopic (XPS) measurements were made using a PHI Quantum 5000 XPS system (USA) with a monochromatic Al Kα source and a charge neutralizer.

2.4. Photocatalysis experiments

The RR2 concentration and temperature in all experiments were 20 mg/L and 298 K, respectively. The photocatalyst dosage was 0.5 g/L in all experiments except those were conducted to determine the effects of dose of 1CBW on RR2 photocatalysis; the solution pH was 3 in all experiments except those were performed to determine the effects of pH on RR2 photocatalysis. In experiments in which scavengers were added, the initial molar concentration of each scavenger equaled the concentration of 0.5 g/L 1CBW. Photocatalysis experiments were conducted in a 3 L glass reactor. A 400 W Xe lamp (200 nm < wavelength < 700 nm, UniVex BT-580, Taiwan) was used to provide simulated solar radiation. The intensity of the light from the lamp was 30.3 mW/ cm^2. A quartz appliance that was filled with 2 M $NaNO_2$ solution was put on the top of the reactor to cut the UV and to provide visible-light [29]. Adsorption experiments were carried out in darkness. The reaction medium was stirred continuously at 300 rpm and aerated with air to maintain suspension. Aliquots, each with a volume of 10 mL, were withdrawn from the reactor at specific time intervals to monitor the progress of the reaction. Following sampling, solids were separated by filtration through a 0.22 μm filter (Millipore, USA), and the RR2 that remained in the filtrate was analyzed by absorbance at 538 nm using a spectrophotometer (Hitachi U-5100, Japan). The photocatalysis efficiency was the difference between the RR2 concentrations before and after each experiment. Some experiments were performed in triplicate and mean values were reported.

3. Results and discussion

3.1. Surface characteristics of CNTs/BW composites

XRD spectra are utilized to examine the crystallization of BW and CNTs/BW composites (Fig. 1). All samples have similar diffraction peaks. The peaks at 28.3°, 32.8°, 47.0°, 55.8°, 76.1°, and 78.6° correspond to the (1 1 3), (2 0 0), (0 2 6), (3 1 3), (3 3 3), and (2 4 0) reflections of the crystal phases,

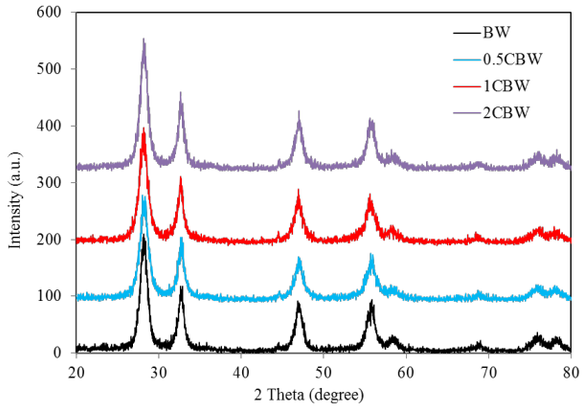

Fig. 1. XRD patterns of CNTs/BW composites.

Table 1
Surface characteristics of prepared photocatalysts

	CNTs*	BW	0.5CBW	1CBW	2CBW
Crystalline size (nm)	–	8.0	7.3	6.8	7.5
BET surface area (m^2/g)	82.2	100.3	97.1	84.1	83.4
Pore diameter (nm)	2.5	10.7	8.5	12.5	12.3
Pore volume (cm^3/g)	1.07	0.29	0.23	0.29	0.27
pH_{zpc}	4.9	2.2	3.5	4.6	3.2
Band gap (eV)	–	3.1	2.7	3.1	3.0

*: Wu [27]

respectively. BW and CNTs/BW composites exhibit good crystallinity; the distinct diffraction peaks correspond to the orthorhombic BW phase (JCPDS no. 73–1126). The peaks at 25.9° and 44.1° correspond to the (0 0 2) and (1 0 0) reflections of the CNTs, respectively [9,10]. The typical peaks of CNTs were not observed in the spectra of the CNTs/BW composites, perhaps because of the small amount of CNTs (weight ratio < 3.5%) and their high dispersion in the CNTs/BW composites. Similar results can be found in the literature for CNTs/TiO_2 [11], CNTs/BW [17], CNTs/$InVO_4$ [15], CNTs/$Bi_4O_5Br_2$ [13] and CNTs/$BiVO_4$/BW [14]. The crystalline sizes of CNTs/BW composites were calculated using the Scherrer equation (not shown) and all were close to that of BW (Table 1), indicating that adding CNTs did not change the crystalline properties of BW. The crystalline size of all prepared photocatalysts was in the range of 6–8 nm.

Table 1 presents the surface characteristics of BW and CNTs/BW composites. The BET surface area followed the order BW > 0.5CBW > 1CBW > 2CBW. Yue et al. [17] found that the BET surface areas of BW and 3% CNTs-BW were 19.63 and 43.32 m^2/g, respectively. All the BET surface areas in this study exceeded that obtained by Yue et al. [17]. Since the BET surface area of BW exceeded that of CNTs herein, the BET surface area declined as the amount of CNT dopant increased (Table 1). Increasing the BET surface area of the photocatalyst increased the number of available adsorption sites, favoring the adsorption of pollutant on the surface of the composite. The increase in adsorption with surface area favored the degradation efficiency of the photocatalyst.

The pH_{zpc} of all CNTs/BW composites exceeded that of BW (Table 1), implying that doping CNTs on BW improved the adsorption of RR2 on the composites.

The absorption spectra of CNTs/BW composites exhibited strong absorption in the visible region at wavelengths of longer than 400 nm, and a red shift occurred upon the addition of CNTs, except in 1CBW (data not shown). The band gaps of BW, 0.5CBW, 1CBW and 2CBW were measured as 3.1, 2.7, 3.1 and 3.0 eV, respectively (Table 1). A narrower band gap is known to be associated with higher photoactivity of the photocatalyst. However, the photocatalytic activity of the photocatalyst was also influenced by its adsorption capacity, which was in turn affected by its BET surface area and pH_{zpc}. Hence, evaluating the photocatalytic activity in terms of only one surface parameter of the photocatalyst was difficult.

Fig. 2a shows an SEM image of 1CBW, which reveals high crystallinity, a high tendency to agglomerate and a rough surface. The TEM image provides insight into the morphology and microstructure of 1CBW (Fig. 2b). BW particles are clearly observed on the surface of the CNTs. The diameters of CNTs and BW in the 1CBW were approximately 25 and 10 nm, respectively. Fig. 3c displays a high-resolution TEM image of 1CBW, which clearly reveals a very close contact interface between the CNTs and BW in the composites, which forms a heterojunction. The strong attachment of CNTs to BW favors the separation of photo-generated electron-hole pairs owing to the excellent mobility of charge carriers on the surface of the CNTs [17].

XPS analysis is used to investigate the valance states and chemical environment of the constituent elements on the surface of 1CBW. Fig. 3 shows the XPS spectra of 1CBW. Two peaks in the Bi_{4f} region (Fig. 3a) at 164.1 and 158.8 eV are attributable to $Bi_{4f5/2}$ and $Bi_{4f7/2}$, respectively [30–33], and are characteristic of Bi^{3+}. The binding energies of 37.2 and 35.0 eV for $W_{4f5/2}$ and $W_{4f7/2}$ are assigned to the W^{6+} oxidation state (Fig. 3b) [31–33]. The O_{1s} region is associated with four peaks. The XPS spectral peaks in the O_{1s} region at 529.9 and 531.7 eV are attributed to Bi-O and W-O, respectively (Fig. 3(c)) [34]. The peak at 531.1 eV indicates the adsorption of hydroxyl groups (OH^-) on the surface of 1CBW [33,35]. The peak at 532 eV is attributed to the C-O bonds [36]. The C_{1s} region is associated with two peaks. The main peak at 284.6 eV is attributed to sp^2-hybridized carbon from the CNTs, and thereby the C-C bond [11,13,17,25,37]. The peak at 285.6 eV corresponds to the C-O bond [11,17].

Most of the PL emission arises from the recombination of photo-generated electrons and holes. PL analysis is performed to elucidate the separation efficiency of photo-generated electron-hole pairs in photocatalysts. Fig. 4 displays the PL spectra of BW and CNTs/BW composites. The intensities of the PL spectra followed the order BW > 2CBW > 1CBW > 0.5CBW. The large fall in PL peak intensities indicated that the combination of photo-induced electrons and holes could be greatly inhibited, increasing the amount of highly reactive species that were available for RR2 photodegradation. This study revealed that the introduction of CNTs considerably inhibited the recombination of photo-generated electron-hole pairs, indicating that the separation of photo-generated electron-hole pairs in CNTs/BW composites was more efficient than in BW. BW is excited

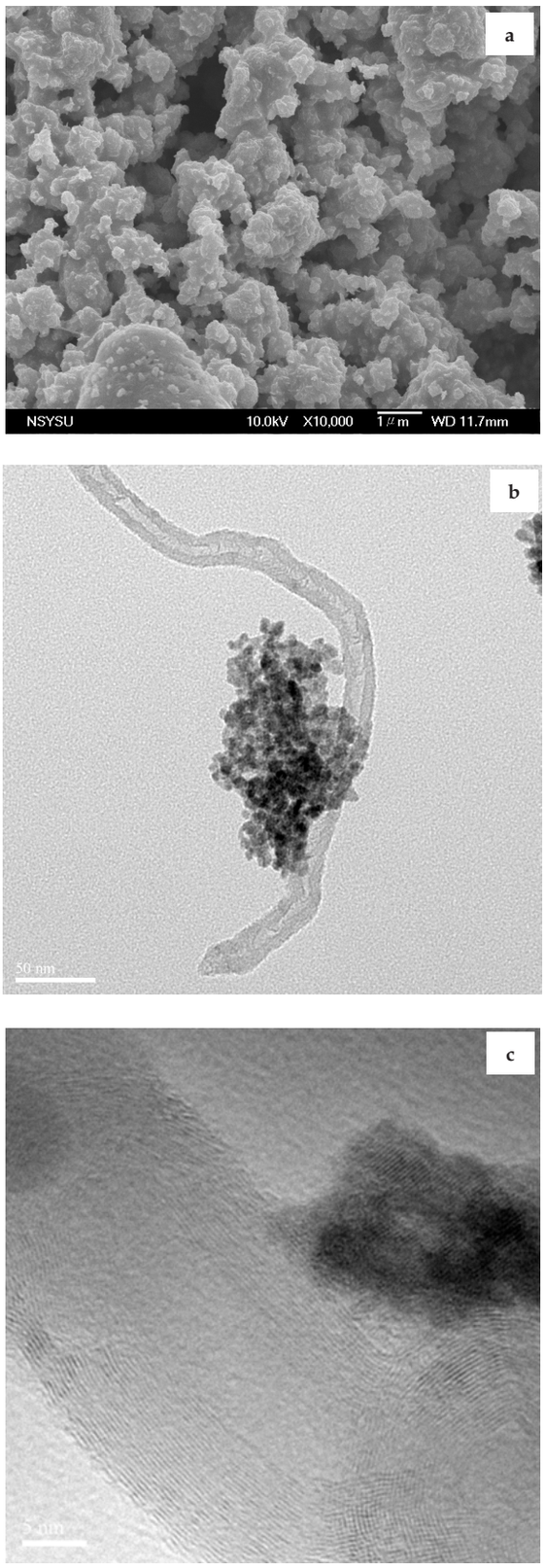

Fig. 2. Micrographs of 1CBW (a) SEM (b) TEM (c) high resolution TEM.

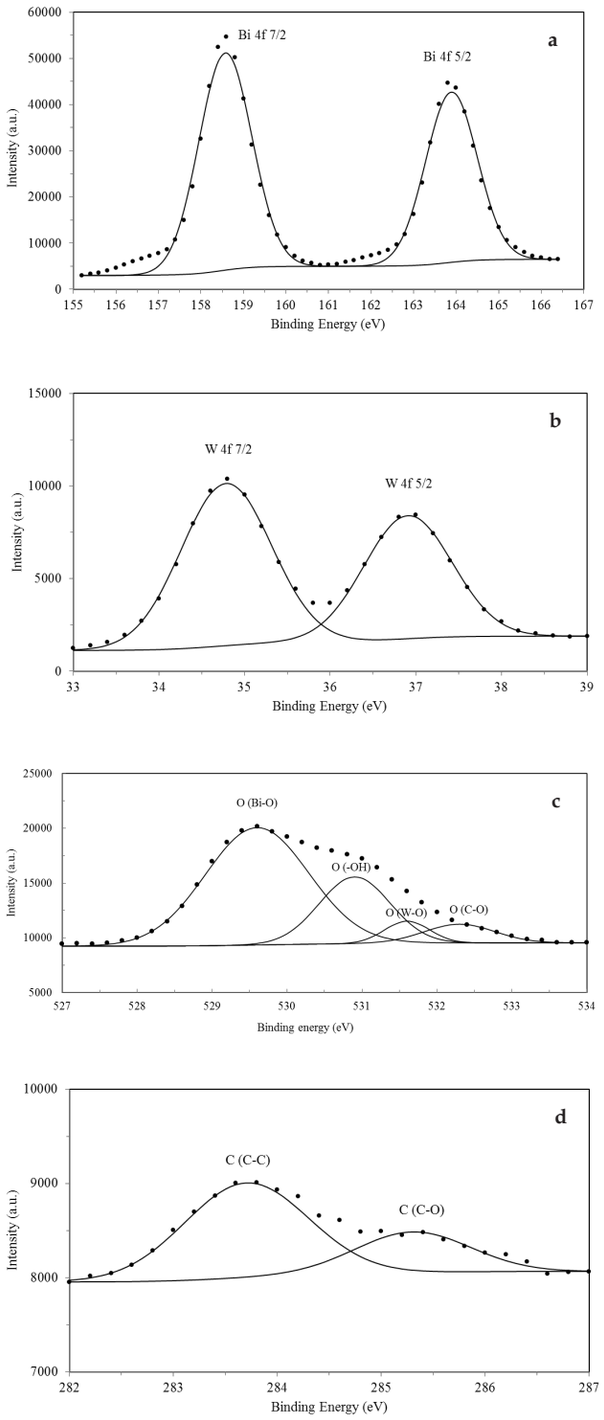

Fig. 3. XPS spectra of 1CBW for (a) Bi_{4f}, (b) W_{4f}, (c) O_{1s}, (d) C_{1s}.

under UV irradiation, and the excited electrons are transported from the conduction band of BW to the CNTs owing to the strong interaction and intimate contact between BW and CNTs, which prevents the direct recombination of electron-hole pairs. The role of CNTs in CNTs/BW composites was the same as in CNTs/$InVO_4$ nanofibers [15].

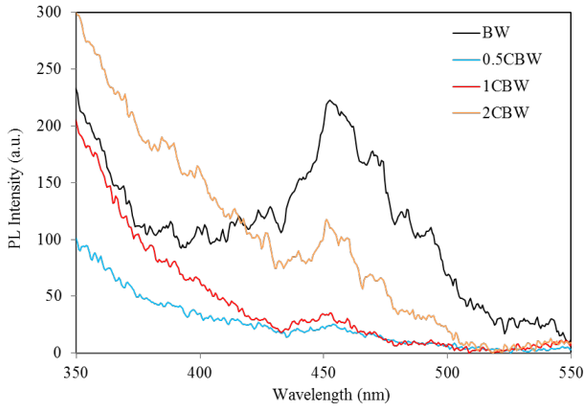

Fig. 4. PL spectra of CNTs/BW composites.

3.2. Determination of photocatalytic activity of CNTs/BW composites

Figs. 5a, 5b and 5c show the removal of RR2 by adsorption, solar photocatalysis and visible-light photocatalysis in various CNTs/BW composites, respectively. After 60 min of reaction, the amounts of RR2 removed by adsorption in BW, 0.5CBW, 1CBW and 2CBW were 17%, 11%, 34% and 26%, respectively; those removed by solar photocatalysis in BW, 0.5CBW, 1CBW and 2CBW were 95%, 74%, 95% and 90%, respectively, and those removed by visible-light photocatalysis in BW, 0.5CBW, 1CBW and 2CBW were 22%, 23%, 45% and 32%, respectively. The adsorption and photocatalysis efficiency of RR2 by various CNTs/BW composites were both highest in 1CBW. The pseudo-first-order equation [Eq. (1)] was used to compare the rates of photocatalysis by photocatalysts [11,17,28].

$$\ln(C/C_0) = -kt \quad (1)$$

where C_0, t and C, are the initial RR2 concentration (mg/L), reaction time, and RR2 concentration at time t (mg/L), respectively, and k is the pseudo-first-order rate constant (h^{-1}). Table 2 lists the RR2 photocatalysis rate constants of BW and CNTs/BW composites. For solar photocatalysis, the k values followed the order 1CBW > BW > 2CBW > 0.5 CBW; for visible-light photocatalysis, the k values followed the order 1CBW > 2CBW > 0.5CBW > BW. Notably, 1CBW exhibited the highest photocatalytic activity of all prepared photocatalysts; moreover, doping with CNTs improved the photocatalytic activity of BW under visible-light. When BW is irradiated by visible-light, the valence electrons are excited into the conduction band (CB), leaving holes in the valance band (VB). When CNTs are incorporated into BW, the photo-generated electron on the CB of BW can be further transferred to the CNTs, effectively inhibiting the recombination of the photo-generated electron-hole pairs. In CNTs/BW composites with a little added CNTs, the CNTs may cover/block the photocatalytic sites, so the photocatalytic activity of 0.5CBW was lower than that of BW. When CNTs/BW composites contain excess CNTs, the CNTs become recombination centers of photo-generated electrons and holes; accordingly, the photocatalytic activ-

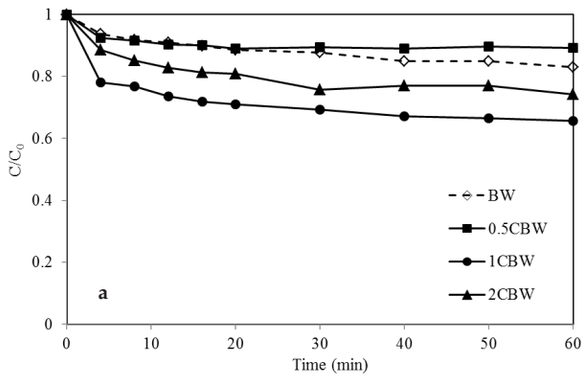

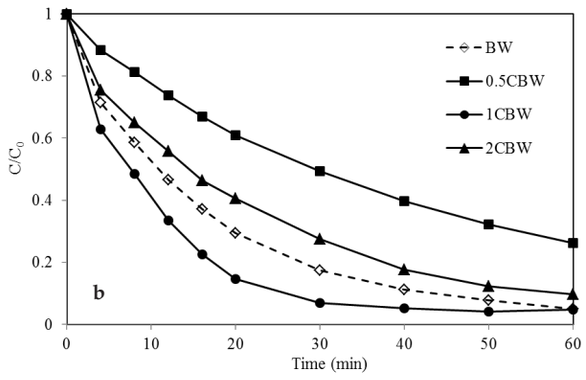

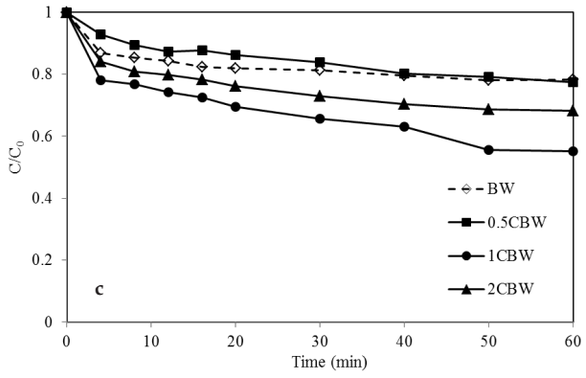

Fig. 5. Removal of RR2 by CNTs/BW composites (a) adsorption (b) solar photocatalysis (c) visible-light photocatalysis ([RR2] = 20 mg/L, [photocatalyst] = 0.5 g/L, pH = 3).

ity of 2CBW was lower than that of 1CBW. 1CBW exhibited the best photocatalytic activity of any of the CNTs/BW composites herein. Yue et al. [17] suggested that increasing the amount of CNTs in such composites blocks their pores and reduces the number of active sites of BW, reducing the photocatalysis efficiency of the photocatalyst. Additionally, the CNTs shield UV light, reducing absorbance in the UV region; hence, doping BW with the appropriate amount of CNTs is the most important issue in the preparation of CNTs/BW composites. With respect to the doping BW with AC, efficiencies of visible-light photocatalysis have been found to follow the order 2% AC/BW > 25% AC/BW > BW > 13% AC/BW [23]. Yue et al. [17] indicated that the photocatalysis efficiencies of various CNTs/BW composites followed the order 3% CNTs-BW > 1.5% CNTs-BW > 0.3% CNTs-BW > BW > 5% CNTs-BW > 10% CNTs-BW. No single rule governs the optimal amount of carbon materials for modifying the surface of BW.

Table 2
RR2 photocatalysis rate constants of prepared photocatalysts

	BW	0.5CBW	1CBW	2CBW
Solar irradiation				
k (h^{-1})	2.86	1.30	5.24 (2.77)* (2.17)**	2.27
R^2	0.995	0.999	0.995 (0.998)* (0.995)**	0.996
Visible-light irradiation				
k (h^{-1})	0.234	0.246	0.438	0.342
R^2	0.971	0.839	0.974	0.971

*: run 2; **: run 3

Fig. 6 presents the effects of 1CBW dose and pH on RR2 removal. After 60 min reaction, the amounts of RR2 photodegraded by 1CBW following the addition of 0.5 and 1 g/L of 1CBW were 95% and 96%, respectively, and the amounts removed by adsorption were 34% and 49%, respectively. The efficiencies of photocatalysis and adsorption of RR2 by 1CBW increased with 1CBW dosage, because the number of available adsorption and photocatalytic sites on the surface of 1CBW increased. The pH of solution affects the adsorption and dissociation of RR2, the 1CBW surface charge, and the oxidation potential of the 1CBW valence band. After 60 min of reaction, the photocatalysis of RR2 by 1CBW at pH 3 and 9 reached 95% and 58%, respectively, and that by adsorption reached 34% and 16%, respectively. RR2 was an anionic dye in solution. The repulsive force between 1CBW and RR2 was stronger at pH 9 than at pH 3 so the photocatalysis and adsorption efficiency at pH 3 were greater than at pH 9. The photocatalysis efficiency of tetracycline increased with pH in the CNTs/BW system [17]. The difference between the trend identified in this study and that identified by Yue et al. [17] may be attributed to the use of different parent compounds.

To identify the active species in the photocatalysis process, scavengers were added to the photocatalysis system: Cr(VI) was used as the photo-generated electron scavenger to determine whether superoxide radicals were present. To trap radicals and holes, Cr(VI) [38,39], EDTA-2Na [30,40] and IPA [30,39,40] were utilized as superoxide radicals, holes and hydroxyl radical scavengers, respectively. Fig. 7 plots the photocatalysis of RR2 by the solar/1CBW system in the presence of various scavengers. After 60 min of reaction, the percentages of RR2 removed in solar/1CBW, solar/1CBW/IPA, solar/1CBW/EDTA-2Na and solar/1CBW/Cr(VI) systems were 95%, 94%, 26% and 79%, respectively. Adding IPA to the RR2 solution slightly reduced the RR2 photocatalysis percentage but adding EDTA-2Na strongly slowed the photocatalysis of RR2. In an aqueous photocatalytic reaction, photo-generated holes react with chemisorbed hydroxyl groups or water to form hydroxyl radicals and the photo-generated electrons interact with adsorbed oxy-

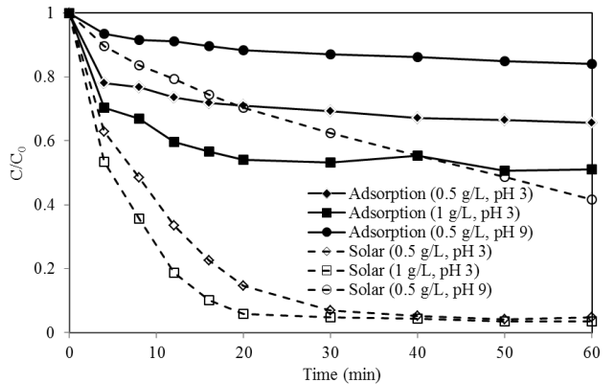

Fig. 6. Effects of photocatalyst dose and pH on RR2 removal.

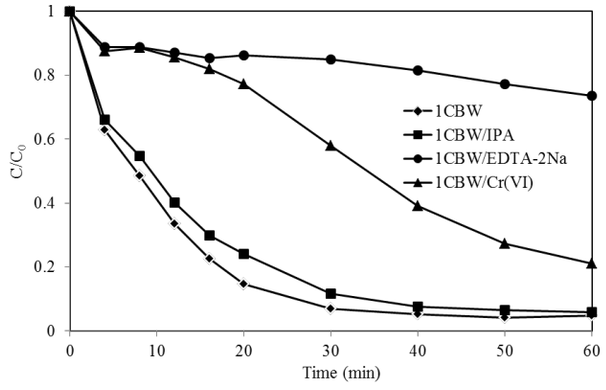

Fig. 7. Photocatalysis of RR2 in solar/1CBW system in the presence of different scavengers.

gen to form superoxide radicals. Both the hydroxyl radicals and the superoxide radicals are strongly oxidative species in the photocatalysis of pollutants [31]. Photocatalytic reactions are well known to proceed on or very near the surface of photocatalysts. In this study, photo-generated holes were generated on the surface of 1CBW and could not spread into the solution; hence, improved adsorption could promote photocatalysis by 1CBW. The photo-generated holes on the surface of BW did not react with OH^-/H_2O to form hydroxyl radicals [28,41]. Moreover, doping CNTs (C/B molar ratio = 1) into BW did not alter its band gap; so hydroxyl radicals were not thought to have been produced in the 1CBW system herein. This investigation suggested that photo-generated holes played a major role and superoxide radicals had a minor role in the photocatalysis of RR2 by 1CBW. Yue et al. [17] suggested that both photo-generated holes and hydroxyl radicals were responsible for photocatalysis in CNTs/BW composites and they used the hydrothermal process to synthesize CNTs/BW composites. The present study suggested that the synthetic method affected the main reactive species, which were responsible for photocatalysis in CNTs/BW composites.

Over three cycles, the proportion of RR2 that was removed by solar/BW at 60 min of reaction decreased from 95% to 72% (data not shown); the corresponding decrease

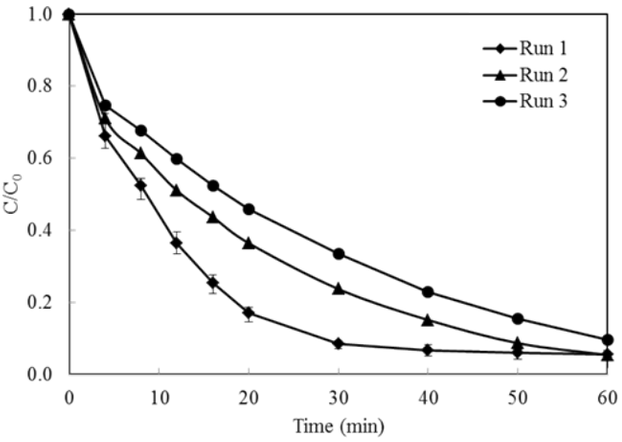

Fig. 8. Profiles of cyclic photocatalysis for RR2 in solar/1CBW system.

for solar/1CBW was 95% to 90% (Fig. 8). The photocatalytic activity of BW and 1CBW declined over three cycles probably because of the residual by-product of RR2 on the surface of photocatalysts, which occupied some of the active sites of the photocatalysts. The k values of solar/BW in runs 1, 2 and 3 were 2.86, 1.11 and 1.09 h^{-1}, respectively, and those of solar/1CBW in runs 1, 2 and 3 were 5.24, 2.77 and 2.17 h^{-1}, respectively. Clearly, the rate of decline of photocatalytic activity in BW exceeded that in 1CBW. This study suggested that doping CNTs on BW improved not only the photocatalytic activity of BW but also the reusability of BW.

4. Conclusions

CNTs/BW composites were successfully synthesized by the single-step solvothermal process and the addition of CNTs did not change the crystalline properties of BW. CNTs, in an appropriate amount, accepted and transported electrons, inhibiting the recombination of electrons with the holes that remained on the surface of BW, improving the photocatalytic activity in CNTs/BW composites in RR2 degradation. Experimental results revealed that doping CNTs on BW enhanced not only their adsorption ability and photocatalytic activity but also their reusability. The efficiencies of photocatalysis and adsorption of RR2 by CNTs/BW composites increased with CNTs/BW composites dosage; conversely, the performances decreased with solution pH value. The experimental results revealed that photo-generated holes played a major role and superoxide radicals had a minor role in the photocatalysis of RR2 by CNTs/BW composites. This study suggested that different synthetic method affected the main reactive species that were responsible for photocatalysis in CNTs/BW composites.

Acknowledgement

The authors would like to thank the National Science Council of the Republic of China, Taiwan, for financially supporting this research under Contract No. MOST 105-2221-E-151-001.

References

[1] A. Kudo, S. Hijii, H_2 or O_2 evolution from aqueous solutions on layered oxide photocatalysts consisting of Bi^{3+} with $6s^2$ configuration and d^0 transition metal Ions, Chem. Lett., 28 (1999) 1103–1104.

[2] Z.J. Zhang, W.Z. Wang, M. Shang, W.Z. Yin, Low-temperature combustion synthesis of Bi_2WO_6 nanoparticles as a visible-light-driven photocatalyst, J. Hazard. Mater., 177 (2010) 1013–1018.

[3] Y. Geng, P. Zhang, S. Kuang, Fabrication and enhanced visible-light photocatalytic activities of $BiVO_4/Bi_2WO_6$ composites, RSC Adv., 4 (2014) 46054–46059.

[4] B. Liu, Z. Wang, S. Zhou, J. He, Synthesis and characterization of a novel $BiVO_4/SiO_2$ nanocomposites, Mater. Lett., 160 (2015) 218–221.

[5] A.K. Geim, Graphene: status and prospects, Science, 324 (2009) 1530–1534.

[6] K.E. Tettey, M.Q. Yee, D. Lee, Photocatalytic and conductive MWCNT/TiO_2 nanocomposite thin films, ACS Appl. Mater. Interf., 2 (2010) 2646–2652.

[7] X. Lu, W.L. Yim, B.H.R. Suryanto, C. Zhao, Electrocatalytic oxygen evolution at surface-oxidized multiwall carbon nanotubes, J. Am. Chem. Soc., 137 (2015) 2901–2907.

[8] J. Wang, Y. Lin, M. Pinault, A. Filoramo, M. Fabert, B. Ratier, J. Boucle, N.H. Boime, Single-step preparation of TiO_2/MWCNT nanohybrid materials by laser pyrolysis and application to efficient photovoltaic energy conversion, ACS Appl. Mater. Interf., 7 (2015) 51–56.

[9] W. Wang, P. Serp, P. Kalck, J.L. Faria, Photocatalytic degradation of phenol on MWNT and titania composite catalysts prepared by a modified sol-gel method, Appl. Catal. B: Environ., 56 (2005) 305–312.

[10] S.H.S. Zein, A.R. Boccaccini, Synthesis and characterization of TiO_2 coated multiwalled carbon nanotubes using a sol gel method, Ind. Eng. Chem. Res., 47 (2008) 6598–6606.

[11] C.H. Wu, C.Y. Kuo, S.T. Chen, Synergistic effects between TiO_2 and carbon nanotubes (CNTs) in TiO_2/CNTs system under visible light irradiation, Environ. Technol., 34 (2013) 2513–2519.

[12] J. Lv, D. Li, K. Dai, C. Liang, D. Jiang, L. Lu, G. Zhu, Multiwalled carbon nanotube supported CdS-DETA nanocomposite for efficient visible light photocatalysis, Mater. Chem. Phys., 186 (2017) 372–381.

[13] J. Di, M. Ji, J. Xia, X. Li, W. Fan, Q. Zhang, H. Li, $Bi_4O_5Br_2$ ultrasmall nanosheets in situ strong coupling to MWCNT and improved photocatalytic activity for tetracycline hydrochloride degradation, J. Mol. Catal. A: Chem., 424 (2016) 331–341.

[14] L. Lin, D. Yu, W. Wang, P. Gao, K. Bu, B. Liu, Preparation of $BiVO_4/Bi_2WO_6$/multi-walled carbon nanotube nanocomposites for enhancing photocatalytic performance, Mater. Lett., 185 (2016) 507–510.

[15] Y. Zhang, D. Ma, J. Wu, Q. Zhang, Y. Xin, N. Bao, One–step preparation of CNTs/$InVO_4$ hollow nanofibers by electrospinning and its photocatalytic performance under visible light, Appl. Surf. Sci., 353 (2015) 1260–1268.

[16] L. Ge, C. Han, Synthesis of MWNTs/g-C_3N_4 composite photocatalysts with efficient visible light photocatalytic hydrogen evolution activity, Appl. Catal. B: Environ., 117–118 (2012) 268–274.

[17] L. Yue, S. Wang, G. Shan, W. Wu, L. Qiang, L. Zhu, Novel MWNTs-Bi_2WO_6 composites with enhanced simulated solar photoactivity toward adsorbed and free tetracycline in water, Appl. Catal. B: Environ., 176–177 (2015) 11–19.

[18] B. Liu, Z. Li, S. Xu, X. Ren, D. Han, D. Lu, Facile in situ hydrothermal synthesis of $BiVO_4$/MWCNT nanocomposites as high performance visible-light driven photocatalysts, J. Phys. Chem. Solids, 75 (2014) 977–983.

[19] C.H. Chen, Y.H. Liang, W.D. Zhang, $ZnFe_2O_4$/MWCNTs composite with enhanced photocatalytic activity under visible-light irradiation, J. Alloy Compd., 501 (2010) 168–172.

[20] J. Chen, G. Li, Y. Huang, H. Zhang, H. Zhao, T. An, Optimization synthesis of carbon nanotubes-anatase TiO_2 composite photocatalyst by response surface methodology for photocatalytic degradation of gaseous styrene, Appl. Catal. B Environ., 123–124 (2012) 69–77.

[21] D. Xu, P. Lu, P. Dai, H. Wang, S. Ji, In situ synthesis of multiwalled carbon nanotubes over $LaNiO_3$ as support of cobalt nanoclusters catalyst for catalytic applications, J. Phys. Chem. C., 116 (2012) 3405–3413.

[22] Y.Y. Li, J.P. Liu, X.T. Huang, J.G. Yu, Carbon-modified Bi_2WO_6 nanostructures with improved photo catalytic activity under visible light, Dalton Trans., 39 (2010) 3420–3425.

[23] S. Murcia-López, J.A. Navío, M.C. Hidalgo, Role of activated carbon on the increased photocatalytic activity of AC/Bi_2WO_6 coupled materials, Appl. Catal. A: Gen., 466 (2013) 51–59.

[24] H. Ma, J. Shen, M. Shi, X. Lu, Z. Li, Y. Long, N. Li, M. Ye, Significant enhanced performance for Rhodamine B, phenol and Cr(VI) removal by Bi_2WO_6 nancomposites via reduced graphene oxide modification, Appl. Catal. B: Environ., 121–122 (2012) 198–205.

[25] Y.L. Min, K. Zhang, Y.C. Chen, Y.G. Zhang, Enhanced photocatalytic performance of Bi_2WO_6 by graphene supporter as charge transfer channel, Sep. Purif. Technol., 86 (2012) 98–105.

[26] Y. Chen, X. Cao, J. Kuang, Z. Chen, J. Chen, B. Lin, The gas-phase photocatalytic mineralization of benzene over visible-light-driven Bi_2WO_6@C microspheres, Catal. Commun., 12 (2010) 247–250.

[27] C.H. Wu, Studies of the equilibrium and thermodynamics of the adsorption of Cu^{2+} onto as-produced and modified carbon nanotubes, J. Colloid Interf. Sci., 311 (2007) 338–346.

[28] C.H. Wu, C.Y. Kuo, J.T. Wu, M.J. Hsu, T.J. Jhang, Photodegradation of C.I. Reactive Red 2 in the Bi_2WO_6 system: Determination of surface characteristics and photocatalytic activities of Bi_2WO_6, React. Kinet. Mech. Catal., 117 (2016) 391–404.

[29] M. Su, C. He, V.K. Sharma, M.A. Asi, D. Xia, X.Z. Li, H. Deng, Y. Xiong, Mesoporous zinc ferrite: synthesis, characterization, and photocatalytic activity with H_2O_2/visible light, J. Hazard. Mater., 211–212 (2012) 95–103.

[30] M.S. Gui, W.D. Zhang, Q.X. Su, C.H. Chen, Preparation and visible light photocatalytic activity of Bi_2O_3/Bi_2WO_6 heterojunction photocatalysts, J. Solid State Chem., 184 (2011) 1977–1982.

[31] Z. Zhang, W. Wang, E. Gao, M. Shang, J. Xu, Enhanced photocatalytic activity of Bi_2WO_6 with oxygen vacancies by zirconium doping, J. Hazard. Mater., 196 (2011) 255–262.

[32] Y. Guo, G. Zhang, H. Gan, Synthesis, characterization and visible light photocatalytic properties of Bi_2WO_6/rectorite composites, J. Colloid Interf. Sci., 369 (2012) 323–329.

[33] Z. Sun, X. Li, S. Guo, H. Wang, Z. Wu, One-step synthesis of Cl^--doped Pt(IV)/Bi_2WO_6 with advanced visible-light photocatalytic activity for toluene degradation in air, J. Colloid. Interf. Sci., 412 (2013) 31–38.

[34] M.S. Gui, W.D. Zhang, Preparation and modification of hierarchical nanostructured Bi_2WO_6 with high visible light-induced photocatalytic activity, Nanotechnol., 22 (2011) 265601.

[35] S. Bai, H. Liu, J. Sun, Y. Tian, S. Chen, J. Song, R. Luo, D. Li, A. Chen, C.C. Liu, Improvement of TiO_2 photocatalytic properties under visible light by WO_3/TiO_2 and MoO_3/TiO_2 composites, Appl. Surf. Sci., 338 (2015) 61–68.

[36] M.H. Ahmed, J.A. Byrne, J.A.D. McLaughlin, A. Elhissi, W. Ahmed, Comparison between FTIR and XPS characterization of amino acid glycine adsorption onto diamond-like carbon (DLC) and silicon doped DLC, Appl. Surf. Sci., 273 (2013) 507–514.

[37] V. Parry, G. Berthome, J.C. Joud, O. Lemaire, A.A. Franco, XPS investigations of the proton exchange membrane fuel cell active layers aging: Characterization of the mitigating role of an anodic CO contamination on cathode degradation, J. Power Sources, 196 (2011) 2530–2538.

[38] Y. Chen, S. Yang, K. Wang, L. Lou, Role of primary active species and TiO_2 surface characteristic in UV-illuminated photodegradation of Acid Orange 7, J. Photochem. Photobiol. A: Chem., 172 (2005) 47–54.

[39] Y. Zhang, C. Shao, X.H. Li, N. Lu, M.Y. Zhang, P. Zhang, X. Zhang, Y. Liu, Controllable synthesis and enhanced visible photocatalytic degradation performances of Bi_2WO_6-carbon nanofibers heteroarchitectures, J. Sol-Gel Sci. Technol., 70 (2014) 149–158.
[40] H. Huang, K. Liu, K. Chen, Y. Zhang, Y. Zhang, S. Wang, Ce and F comodification on the crystal structure and enhanced photocatalytic activity of Bi_2WO_6 photocatalyst under visible light irradiation, J. Phys. Chem. C., 118 (2014) 14379–14387.
[41] Y. Fu, C. Chang, P. Chen, X. Chu, L. Zhu, Enhanced photocatalytic performance of boron doped Bi_2WO_6 nanosheets under simulated solar light irradiation, J. Hazard. Mater., 254–255 (2013) 185–192.